Efficient Fourier-Based Evaluation of SAR Focusing Kernels

Pau Prats-Iraola, German Aerospace Center (DLR), Pau.Prats@dlr.de, Germany
Marc Rodriguez-Cassola, German Aerospace Center (DLR), Marc.Rodriguez@dlr.de, Germany
Francesco De Zan, German Aerospace Center (DLR), Francesco.DeZan@dlr.de, Germany
Paco López-Dekker, German Aerospace Center (DLR), Francisco.LopezDekker@dlr.de, Germany
Rolf Scheiber, German Aerospace Center (DLR), Rolf.Scheiber@dlr.de, Germany
Andreas Reigber, German Aerospace Center (DLR), Andreas.Reigber@dlr.de, Germany

Abstract

This contribution addresses the efficient evaluation of Fourier-based kernels for synthetic aperture radar (SAR) image formation. The goal is to evaluate the quality of the focused impulse response function and the residual phase errors of the kernel without having to implement the processor itself nor perform a costly point-target simulation followed by the processing. The proposed methodology is convenient for situations where the assumption of a hyperbolic range history does not hold anymore, and hence a compact analytic expression of the point target spectrum is not available. Examples where the hyperbolic range history does not apply include very high-resolution spaceborne SAR imaging or bistatic SAR imaging. The approach first computes numerically the two-dimensional (2D) spectrum of a point target and then uses the transfer function of the focusing kernel to match it, and hence obtain the impulse response function (IRF). The methodology is validated by comparing the matched IRFs with the ones obtained using point-target simulations.

1 Introduction

Future spaceborne synthetic aperture radar (SAR) systems are being developed in order to deliver a better performance, e.g., in terms of spatial resolution and coverage. The use of satellite constellations is also an intense research topic, where bistatic imaging can help to further improve the aforementioned aspects. In terms of the SAR raw data focusing, high resolution and bistatic imaging are demanding, especially when the range history can no longer be expressed analytically in a compact form. In such cases, the evaluation of the focusing algorithm is usually performed via time-domain simulation of point targets followed by the processing of the raw data using the implemented focusing kernel. This is expensive in computational terms, which also limits the number of scenarios that can be simulated. However, during the assessment of a spaceborne SAR mission, it is desirable to efficiently validate the performance of the focusing kernel for all possible scenarios, e.g., different incidence angles or scene sizes, in order to finally select the most appropriate kernel both in terms of quality and efficiency.

This paper presents a methodology to quantify the performance of a focusing kernel without having to implement the processor itself nor perform a costly point-target simulation. The methodology is based on the computation of the transfer function of the focusing kernel, and hence convenient for Fourier-based processing algorithms. This transfer function is compared to the frequency responses of the point targets, which are computed numerically using their range histories. The difference can be directly evaluated to assess the performance of the focusing kernel. The methodology is valid as long as a large time-bandwidth product applies, which is the usual case in current air- and spaceborne SAR systems. The same rationale was presented in [1] by deriving the transfer function of several kernels analytically. Such analytic evaluation assumes a single-platform linear-track geometry, which is not a valid model for many future SAR missions, e.g., bistatic or very high resolution. For this reason we introduce in this paper the numerical evaluation of the kernel. It is important to remark that for the presented methodology it is not relevant how some steps within the processing are performed. For example, the fact that the chirp scaling algorithm equalizes the range curvatures using the chirp scaling principle, or that an interpolation is implemented via chirp-Z transform, will not affect the transfer function itself, since it is assumed that these steps are performed with arbitrary accuracy. Similarly, pre- and post-processing steps in order to handle spectral or time aliasing, as it happens in the spotlight, ScanSAR, or TOPS modes, are not meant to be evaluated with the proposed approach, as again there is no reason not to perform these steps accurately.

Section 2 expounds the main aspects of the proposed approach, namely, the computation of the point target's spectrum, the evaluation of the transfer function of the focusing kernel, and the spectral support, while Section 2.2 validates it using time-domain point-target simulations.

2 Evaluation of the Focusing Kernel

2.1 Point Target's Spectrum

In order to compute analytically the two-dimensional (2D) spectrum of a range-compressed point target, the first step is a Fourier transform (FT) in the range dimension. This FT, neglecting the amplitude terms, is given by

[2]

$$H(f_{\mathrm{r}}, t_{\mathrm{a}}) = \exp\left[-\mathrm{j}\cdot\frac{2\pi}{\mathrm{c}}\cdot(f_0+f_{\mathrm{r}})\cdot R(t_{\mathrm{a}})\right], \quad (1)$$

where f_{r} is the range frequency, t_{a} is the azimuth time, c is the speed of light, f_0 is the central frequency, and $R(t_{\mathrm{a}})$ is the two-way range history. The azimuth FT can then be computed asymptotically using the principle of stationary phase, which requires the computation of the stationary time, t_{a}^*, being the one satisfying [2]

$$\left.\frac{\partial R(t_{\mathrm{a}})}{\partial t_{\mathrm{a}}}\right|_{t_{\mathrm{a}}=t_{\mathrm{a}}^*} = -\frac{\mathrm{c}\cdot f_{\mathrm{a}}}{f_0+f_{\mathrm{r}}}, \quad (2)$$

where f_{a} is the azimuth frequency. After evaluating (2) for each point of the 2D spectrum, the phase of the FT of (1) can be approximated by

$$\varphi(f_{\mathrm{r}}, f_{\mathrm{a}}) \approx -\frac{2\pi}{\mathrm{c}}\cdot(f_0+f_{\mathrm{r}})\cdot R(t_{\mathrm{a}}^*) - 2\pi\cdot f_{\mathrm{a}}\cdot t_{\mathrm{a}}^*, \quad (3)$$

where the range history needs to be evaluated at each t_{a}^*. In some special cases t_{a}^* can be solved analytically, e.g., when the range history is hyperbolic, which results in the well-known compact expression of the 2D phase spectrum [1, 2]. However, for the cases under consideration in this paper, (2) needs to be solved numerically using, e.g., the Newton-Rapshon method, or series reversion by first expressing $R(t_{\mathrm{a}})$ as a power series of t_{a} [3]. Under the assumption that $\varphi(f_{\mathrm{r}}, f_{\mathrm{a}})$ is an accurate computation of the target's 2D spectrum phase, any processing kernel can be evaluated by comparing its transfer function to that of the point target, as shown in the following section.

2.1.1 Transfer Function of the Kernel

The transfer function can be obtained either from the expressions of the processor found in the literature, or by computing it in case of numerical kernels. Note that Fourier-based SAR image formation is based on phasor multiplications and interpolations, so that a generic transfer function of a Fourier-based focusing kernel can be expressed as follows

$$\begin{aligned} H_{\mathrm{K}}(f_{\mathrm{r}}, f_{\mathrm{a}}) \quad = \quad & W(f_{\mathrm{r}}, f_{\mathrm{a}})\cdot\exp\left[\mathrm{j}\cdot\varphi_{\mathrm{K}}(f_{\mathrm{r}}, f_{\mathrm{a}})\right] \\ & \cdot\ \exp\left[\mathrm{j}\cdot 2\pi\cdot\Delta t_{\mathrm{r}}(f_{\mathrm{a}})\cdot f_{\mathrm{r}}\right] \\ & \cdot\ \exp\left[\mathrm{j}\cdot\varphi_{\mathrm{ac}}(f_{\mathrm{a}})\right], \end{aligned} \quad (4)$$

where $W(\cdot)$ represents the weighting function for sidelobe suppression, and $\varphi_{\mathrm{K}}(\cdot)$ is the matched filter at the given range including the range cell migration correction (RCMC) and higher order terms. The phase ramp of the second exponential term with Δt_{r} represents an interpolation in the range-time, azimuth-frequency domain to correct for any residual term of the range cell migration (RCM). The last exponential term with φ_{ac} represents a residual azimuth compression. The last two might be needed depending on the geometry and the selected processing approach, as for example occurs in the spaceborne case due to the dependence on the effective velocity with range [2]. Equation (4) does not take into account the range dependence on the transfer function, which is addressed in detail in Section 2.1.2. Note also that in (4) the dependence on the target position, (r_0, t_0), has been omitted for simplicity, being r_0 the closest approach distance and t_0 the zero-Doppler time at closest approach.

Operations not performed in the 2D frequency domain need to be considered differently. It has already been shown how to handle interpolations in the fast-time domain. Azimuth-independent phase corrections are also trivial to map, while azimuth-variant phase corrections need to be specially treated. Consider a correction in the slow-time domain given by $\alpha(t_{\mathrm{a}}; f_{\mathrm{r}})$, which might depend on the range frequency. If the correction is very slow variant, one can assume that the stationary phase point computed with (2) will not change significantly. In this case, the correction in the 2D frequency domain is directly given by $\alpha(t_{\mathrm{a}}^*; f_{\mathrm{r}})$. However, a more precise approach is to compute a new stationary phase point, $t_{\mathrm{a}}^\star$, so that (2) is substituted by

$$\left.\frac{\partial}{\partial t_{\mathrm{a}}}\left\{-\frac{2\pi}{\mathrm{c}}\cdot(f_0+f_{\mathrm{r}})\cdot R(t_{\mathrm{a}}) + \alpha(t_{\mathrm{a}}; f_{\mathrm{r}})\right\}\right|_{t_{\mathrm{a}}=t_{\mathrm{a}}^\star} = 2\pi\cdot f_{\mathrm{a}}, \quad (5)$$

and the target phase in the 2D frequency domain is obtained analogously as in (3) using $t_{\mathrm{a}}^\star$ and adding the contribution $\alpha(t_{\mathrm{a}}^\star; f_{\mathrm{r}})$. Finally, the phase error, φ_{error}, is directly obtained by subtracting the phase given by (4) to the computed phase of the target given by (3).

2.1.2 Spectral Support

The impulse response function (IRF) is given by the phase error and the selected weighting. However, the transfer function in (4) does not consider the range-variant property of the geometry. Indeed, such a matched filter will focus a target at the given range, but other targets will be more defocused, the larger their distance to the reference one. Accurate SAR processors accommodate the range-variant geometry, a step that warps the spectrum and, consequently, defines the spectral support of the focused image. Taking as example the range-Doppler algorithm, its azimuth compression filter changes with range, which introduces a Doppler-dependent phase ramp in the fast time, and hence an azimuth-frequency-dependent shift in the range-frequency domain [4], which curves the spectrum of the target. It is even clearer to visualize this effect through the ω-k algorithm, since the Stolt mapping performs this warp directly through an interpolation. Note though, that the main contribution in the shift of the range spectrum comes from the range-variant azimuth compression filter, resulting in a range spectral shift given by

$$\Delta f_{\mathrm{r}}(r, f_{\mathrm{a}}) = \frac{\mathrm{c}}{2\pi}\frac{\partial\varphi_{\mathrm{ac}}(r, f_{\mathrm{a}})}{\partial r}, \quad (6)$$

where r is the range vector. A low-order interpolator can be used to interpolate the phase values and the envelope separately.

An aspect affecting only the spectrum envelope is the wavelength dependence and the truncation of the raw data in time-domain. Indeed, considering an equivalent antenna pattern that falls to zero at half of the beamwidth, the raw data spectrum of a stripmap acquisition is square, but that of a spotlight acquisition is a trapezoid. This can be shown by recalling the well-known relation of the antenna beamwidth with the wavelength and the azimuth antenna length, $\theta_{\mathrm{a}} \propto \lambda / L_{\mathrm{a}}$, where a linear dependence on the wavelength is assumed to be valid. This relation implies that, since the antenna length is fixed, it "sees" the target first at lower frequencies than at higher ones. Precisely due to this wavelength dependence, it can be stated that the nominal azimuth resolution of a stripmap SAR is half of the antenna length. This fact implies automatically that the raw data spectrum *must* be square for a stripmap acquisition. However, as soon as the data are truncated in the slow-time domain, as it happens for example in a spotlight acquisition, the azimuth instantaneous bandwidth is wavelength dependent, resulting in the trapezoidal form of the azimuth spectrum. Indeed, a time-domain simulation of a point target usually neglects the wavelength dependence of the antenna beam, yielding the trapezoidal form that can often be seen in the literature, which is only strictly correct for the spotlight mode. The first two columns of **Figure 1** show the shape of the spectrum at raw- and image-data levels for the stripmap and spotlight modes, where in the latter case the trapezoidal form due to time truncation can be appreciated.

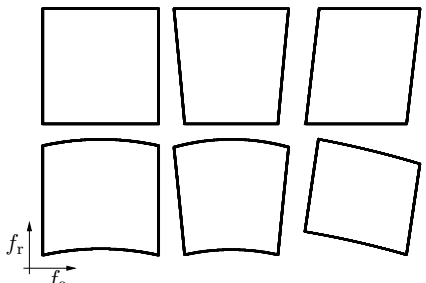

Figure 1: Spectral support at (top row) raw data level and (bottom row) image level for (left column) non-squinted stripmap, (middle column) non-squinted spotlight and (right column) squinted stripmap.

A final aspect that only affects the envelope of the spectrum results from the relation between Doppler frequency and time given by

$$f_{\mathrm{DC}} = -\frac{1}{\lambda} \cdot \frac{\partial R(t_{\mathrm{a}})}{\partial t_{\mathrm{a}}}\Big|_{t_{\mathrm{a}}=t_{\mathrm{c}}}, \tag{7}$$

where t_{c} is the beam-center time. In the monostatic case, eq. (7) takes the well-known expression of $f_{\mathrm{DC}} = 2 \cdot v_{\mathrm{p}} \cdot \sin\beta / \lambda$, where β is the squint angle and v_{p} is the platform velocity. Due to the wavelength dependence, the raw data spectrum is skewed [5]. This is shown in the third column of Figure 1, where the spectral support of a squinted stripmap acquisition is sketched before and after image formation.

2.1.3 Evaluation of the Results

Once the residual phase has been shaped, it can be put into an exponential term and an inverse FT will result in the IRF for the point being evaluated, i.e.,

$$h(t_{\mathrm{r}}, t_{\mathrm{a}}) = \mathrm{FT}_{\mathrm{2D}}^{-1}\left\{\Gamma\left\{W(f_{\mathrm{r}}, f_{\mathrm{a}}) \cdot \exp\left[\mathrm{j} \cdot \varphi_{\mathrm{error}}\right]\right\}\right\}, \tag{8}$$

where the $\Gamma\{\cdot\}$ operator represents the shaping of the spectrum expounded in the previous section. The usual parameters of interest can now be measured, namely, resolution, peak-to-sidelobe ratio, integrated-sidelobe ratio, pixel-shift error, etc. The phase value at the maximum of the IRF gives the (interferometric) phase error, which should be ideally 0°.

Table 1: Spotlight and bistatic simulation parameters

Parameter	Spotlight	Bistatic
Central frequency	9.65GHz	9.65GHz
Integration time	~ 8 sec	~ 3 sec
Total az. proc. bandwidth	33 kHz	7 kHz
Azimuth resolution	19 cm	23 cm
Chirp bandwidth	1.2 GHz	150 MHz
Ground range scene size	5 km	2.5 km
Azimuth scene size	5 km	500 m
Spacecraft incidence angle	55°	51°
Aircraft incidence angle	–	45°
Aircraft velocity	–	90 m/s
Aircraft altitude	–	2180 m

2.2 Experimental Validation

This section demonstrates the methodology by comparing its output with time-domain point-target simulations followed by the *true* processing. Two different examples are shown: a monostatic spotlight geometry, and an airborne-spaceborne bistatic geometry (see **Table 1**).
Due to the high resolution of the spotlight example, conventional kernels assuming a hyperbolic range history do not achieve a satisfactory focusing performance. For this reason, the orbit compensation suggested in [6] is used. The range-Doppler and the ω-k approaches are then evaluated, where the latter has been adapted to the spaceborne scenario [7]. Due to the orbit compensation, which is a phase correction performed in the azimuth-time, range-frequency domain, the target's spectrum was computed using (5). The true processing was performed using subapertures and a spectral analysis (SPECAN) approach was used for the azimuth processing [8]. **Figure 2** shows the obtained IRFs and phase errors of the target located at far range at the edge of the scene. The difference in the phase error in the 2D frequency domain between the proposed methodology and the true processing is practically zero, but for the Gibbs phenomenon at spectrum edges. The computation of the IRFs for the nine targets located in the scene took less than a minute with the proposed approach, while the true processing lasted more than four hours in a sixteen-core computer. Note that the size of

the target's spectra and the corresponding matched filters computed with the proposed methodology was just 64×64 pixels and the target's range history was fit with a sixth order polynomial before performing series reversion.

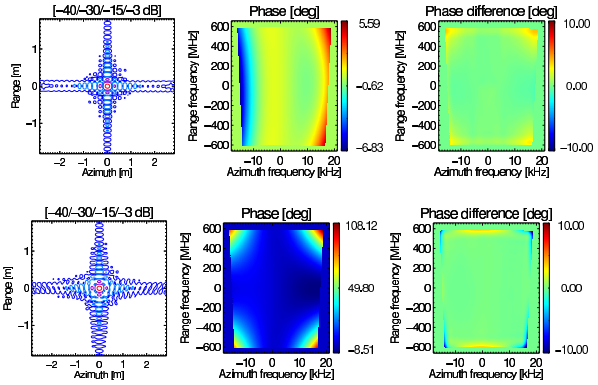

Figure 2: Comparison between the proposed methodology and the time-domain simulation followed by the true processing for the spotlight example (see Table 1). The target is located 2.5 km away from scene center in the azimuth and ground range dimensions. (Left column) contour plot of the simulated IRF. (Middle column) Computed phase error in the 2D frequency domain (in degrees). (Right column) Phase difference between the proposed methodology and the true processing (in degrees). The plots correspond to (top row) EOK [7] and (bottom row) range-Doppler processors, respectively.

Concerning the bistatic example, its geometry corresponds to the experiment that took place on November 2007 between the TerraSAR-X satellite and DLR's F-SAR airborne system [9]. The selected kernel is a numerical range-Doppler algorithm, where the point of stationary phase has been computed using series reversion [3]. Despite being a monochromatic algorithm, it performs well due to the small swath and relative small bandwidth. However, the azimuth-variant characteristic of the survey is not accommodated. **Figure 3** shows the result for a target located at the same range as the reference target but 125 m away from it in the azimuth dimension. Again, the obtained result compared to the true processing is practically identical.

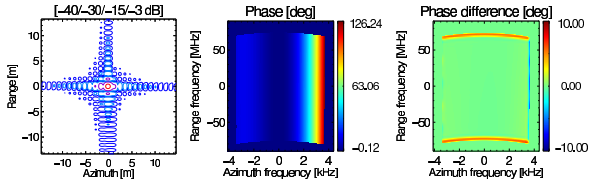

Figure 3: Comparison between the proposed methodology and the time-domain simulation followed by the true processing for the bistatic example (see Table 1). The target is located 125 m away from scene center in the azimuth dimension. (Top left) Contour plot, (top right) phase error of the kernel in the 2D frequency domain (in degrees), and (bottom) phase difference between the proposed methodology and the true processing (in degrees).

3 Conclusions

This paper has presented a methodology to efficiently evaluate the performance of Fourier-based SAR focusing kernels. Such a methodology is convenient for imaging geometries where a close-form analytic expression of the signal in the two-dimensional frequency domain is not possible, as for example occurs in bistatic or very high resolution spaceborne geometries. Due to its high efficiency, it is straightforward to evaluate different mission scenarios, e.g., different latitudes and incidence angles, different spaceborne constellations, or to quantify other aspects like the influence of the topography or the azimuth-variant geometry. The outcome is a global performance of the focusing kernel, hence becoming a powerful tool for the final selection of the focusing kernel that best suits the mission requirements. Additionally, the concept can be exploited to develop and efficiently test new focusing kernels. Furthermore, considering that here only the basic idea has been presented, it is straightforward to extend the concept in order to include further aspects like system effects (e.g., replica, antenna pattern), atmospheric effects, the platform motion in the airborne case, etc.

A high resolution spotlight spaceborne geometry and a hybrid bistatic geometry have been used to validate the proposed approach. In both cases the computed responses were practically identical to those obtained with time-domain simulations followed by the true processing.

References

[1] R. Bamler, *A comparison of range-doppler and wavenumber domain SAR focusing algorithms*, IEEE Trans. Geosci. Remote Sens., vol. 30, no. 4, 1992

[2] I. G. Cumming, F. H. Wong, *Digital Processing of Synthetic Aperture Radar Data. Algorithms and Implementation*, Boston, London: Artech House, 2005

[3] Y. L. Neo *et.al.*, *A Two-Dimensional Spectrum for Bistatic SAR Processing Using Series Reversion*, Geosci. Remote Sens. Lett., vol. 4, no. 1, 2007

[4] G. Fornaro, *et.al.*, *Role of processing geometry in SAR raw data focusing*, IEEE Transactions Aerospace and Elec. Systems, vol. 38, no. 2, 2002

[5] G. W. Davidson and I. Cumming, *Signal Properties of Spaceborne Squint-Mode SAR*, IEEE Trans. Geosci. Remote Sens., vol. 35, no. 3, 1997

[6] P. Prats-Iraola *et.al.*, *High precision SAR focusing of Terrasar-X experimental staring spotlight data*, Proc. IGARSS, Munich, Germany, 2012

[7] A. Reigber *et.al.*, *Extended wavenumber domain SAR focusing with integrated motion compensation*, IEE Proc. Radar Sonar Navig., vol. 153, no. 3, 2006

[8] J. Mittermayer *et.al.*, *Spotlight SAR Data Processing using the Frequency Scaling Algorithm*, IEEE Trans. Geosci. Remote Sens., vol. 37, no. 5, 1999

[9] M. Rodriguez-Cassola *et.al.*, *Bistatic TerraSAR-X/F-SAR spaceborne–airborne SAR experiment: description, data processing, and results*, IEEE Trans. Geosci. Remote Sens., vol. 48, no. 2, 2010